This is the accepted version of the article A.V. Bosisio *et al*., " On the Use of Microwave Radiometers for Deep Space Mission Applications by Means of a Radiometric-Based Scalar Indicator," in *IEEE Journal of Selected Topics in Applied Earth Observations and Remote Sensing*, vol. 8, no. 9, pp. 4336-4344, Sept. 2015, which has been published in final form at https://doi.org/10.1109/JSTARS.2015.2443174

On the Use of Microwave Radiometers for Deep Space Missions Applications by Means of a Radiometric–based Scalar Indicator

Ada Vittoria Bosisio
National Research Council of Italy, CNR/IEIIT
Milano, Italy
adavittoria.bosisio@ieiit.cnr.it

Alberto Graziani
ICTEAM, Université catholique de Louvain,
Louvain-la-Neuve, Belgium
alberto.graziani@uclouvain.be

Vinia Mattioli
HE Space Operations GmbH,
Darmstadt, Germany
vinia.mattioli@eumetsat.int

Paolo Tortora
DIN, University of Bologna
Forlì, Italy
paolo.tortora@unibo.it

Abstract

The estimation of the path delay due to water vapor is a crucial aspect for the calibration of the Doppler observables of a deep space probe. The Advanced Water Vapor Radiometer (AWVR) developed by the Jet Propulsion Laboratory (JPL, NASA) already proved its capability to accurately estimate the path delay during the entire Cassini mission. Here, from the AWVR measurements, a scalar Sky Status Indicator (*SSI*) was developed as a criterion for selecting the radiometric path delay estimations in the orbit determination process. Results indicate that the use of such index allows a reduction of the range rate residual root mean square (RMS).

I. INTRODUCTION

Many works demonstrate the advantages of employing ground-based microwave radiometers (MWRs) over a variety of environmental and engineering applications, including meteorological observations and forecasting [1-3], communications [4-5], geodesy and long-baseline interferometry [6], satellite validation [7], climate [8], fundamental molecular physics [9] and deep space radioscience experiments [10]. Reasons for the utility of MWRs measurements, in particular at 23.8 and 31.4 GHz, are their sensitivity to the atmospheric water vapor and cloud liquid, and their reliability for the accurate estimation of the integrated quantities of those parameters, namely the integrated precipitable water vapor (*IWV*) and the integrated cloud liquid water content (*LWC*). Specifically, accuracy is about 0.4 mm for *IWV* and 0.02 mm for *LWC* [11-12]. An additional important feature of MWRs is the nearly continuous observational capability on time scales of seconds to minutes.

In the framework of deep space probe navigation and radio science experiments, the assessment of the troposphere path delay plays a crucial role since it is one of the main error sources of the deep space observables [13]. Among the different techniques available to estimate the troposphere path delay, the use of MWRs is the most accurate one to estimate the component due to water vapor [14]. The Solar Conjunction Experiment 1 (SCE1) [10], carried out during the cruise phase of the NASA/ESA/ASI Cassini mission to Saturn, demonstrated the importance of an accurate estimation of the tropospheric path delay, particularly, if the solar plasma noise is removed with the so-called multi frequency link [15].

To account for the troposphere path delay, NASA's Deep Space Network (DSN) complexes are equipped with the so-called Tracking System Analytic Calibration (TSAC). As detailed in [16], TSAC is the standard automated troposphere calibration system developed at JPL for deep space probe navigation purposes, which relies on the zenith path delay estimates derived from Global Positioning System (GPS) observations.

To support Cassini's cruise radio science experiments, a new generation of media calibration systems was developed by JPL, the Advanced Media Calibration (AMC) system consisting of an Advanced Water Vapor Radiometer (AWVR), a surface meteorological station (SM) and a microwave temperature profiler (MTP). Two AMC units were developed; one is installed at the Goldstone Deep Space Network (DSN) complex, USA, close to the DSS 25 (Deep Space Station), and the other is at the Robledo DSN complex, Spain, close to the DSS 55. The accuracy of the TSAC calibrations to estimate up to 90% of the zenith path delay is sufficient to solve the Orbit Determination (OD) problem [13] for probe navigation purposes. On the other hand, a higher precision of the solution of the OD problem is required for scientific purposes. In this case, although the TSAC calibration could be applied, the AMC calibration may be the preferred choice, according to its availability at the DSN site. Indeed, the AMC gives intrinsically more precise slant wet path delay (SPD) estimation along the line-of-sight (LOS), notwithstanding its use is still limited in radio science experiments due to the poor performance in cloudy/rainy scenarios compared to the GPS-based estimation.

The present study aims at addressing the use of the AMC approach with respect to the TSAC through the implementation of an atmospheric index, a scalar quantity named Status Sky Indicator (*SSI*) [18], based on the radiometer measurements. The *SSI* capability of validating the use of AMC retrieved path delay in the calibration of the deep space navigation observables is addressed by analyzing the quality of Cassini's range rate residuals obtained using different troposphere calibration datasets. The probe velocity with respect to the Earth (the so-called range rate) was reconstructed by means of precise measurements of the Doppler shift of a highly stable microwave radio link between Cassini and the ground station antennas of NASA's DSN. The root mean square (RMS) of the AMC-based range rate residuals was computed and compared to the one obtained through the standard TSAC procedure. A reduction of the RMS of the residuals gives a clear

indication that the advanced calibration process is more effective than the standard one in estimating the troposphere path delay.
The remainder of this paper is organized as follows: in Section II an overview of the process of the Cassini gravitational flybys and its dataset for the study is given; in Section III, the *SSI* algorithm development and the methodology of its application are explained. In Section IV, results of the analysis on the range rate observable residuals are presented, and finally, in Section V conclusions are discussed.

II. CASSINI GRAVITATIONAL FLYBYS DATASET

The comparison of the AMC and TSAC approaches relies on the range rate residuals of the OD solution computed on a set of gravitational flybys of Saturn and some of its icy moons acquired during the tour phase of the Cassini mission to estimate the gravity field of the target body [19-20]. The following subsections describe briefly the main systems and dataset used in our study.

A. Selected Cassini's Flybys and Orbit Determination Process

For the typical geometry of the flybys, the tracking of Cassini may require up to two or three consecutive Earth days. In this time, the three NASA DSN complexes track the spacecraft and the involved stations may collect more than one pass per flyby. In our study, we used the flybys collected at the DSS 25 antenna at Goldstone. Table I reports the list of the 10 selected flybys with the date of the event and the number of passes available for each flyby. For all the selected cases, our data set is represented by TSAC time series (§II.B), the AMC time series (§II.C) and the two OD solutions obtained calibrating the Cassini observables with the two mentioned techniques.
As far as the OD solutions are concerned, these are computed with the NASA JPL Orbit Determination Program (ODP) [21-22]. For clarity, a brief description of ODP process is reported here. The software computes the least square difference between the deep space observables, received from the spacecraft and properly weighted by a scalar factor, and the observables computed by a detailed mathematical model. In this process, the troposphere calibration enters as one of the errors affecting the computed observables. The effect of the calibration is visible in the residuals of the least square filtering.

B. TSAC measurements

TSAC is the troposphere path delay calibration system developed by JPL to support the tracking and navigation activities of the interplanetary spacecraft [16]. It represents the most reliable and low-cost system capable to provide continuous zenith troposphere calibration for interplanetary spacecraft. According to the current tracking profile, appropriate mapping functions are used to map the zenith path delay along the spacecraft LOS. TSAC calibration is obtained by processing with the JPL GIPSY-OASIS II software [23] the GPS observables collected with a geodetic dual-frequency GPS receiver installed at each DSN complex.
The TSAC zenith tropospheric delay is then divided into its wet and hydrostatic components, by using surface barometric pressure measurements. Additionally, zenith wet and hydrostatic path delay time series are fitted by polynomials to facilitate interpolation in time. Zenith path delay polynomials are specific for each complex and typically have a time span of 6 hours. In our work, the most accurate TSAC zenith path delay estimations are used for the calibration of the analyzed Cassini flybys.

C. AMC measurements

In the AMC unit, the AWVR represents the core of the system: it is an ultra-stable microwave radiometer with steerable antenna capable to point to the spacecraft position in the sky. The AWVR is

a three-channel radiometer with observing channels at 22.2 GHz, 23.8 GHz and 31.4 GHz, with a long-term stability of 10 mK on time scale of 10000 s. It has an off-axis antenna with a beam width of 1 deg and very low side lobes. A detailed description of the instrument is given in [17]. Two retrieval algorithms [24-25] estimate the troposphere path delay combining the measurements of the AWVR, MTP and SM.

The operation of the AMC unit is enabled via scripts and pointing predictions for the AWVR. The use of quality flags is available together with the retrieved path delay to represent both the status of the instrument and the retrieved parameters. The computed flags are: *ZPD* for the zenith path delay retrieval, *WND* for the wind, *SUR* for the SM, *MTP* for the MTP, *WVR* for the AWVR and *CLD* for the presence of clouds which is based on the retrieval of the liquid water *LWC*. For all the flags, a zero value means that the parameter is in the expected range or that the instrument is correctly working. On the other hand, a different value (typically 1) indicates that parameters are out of the proper range or instruments malfunctioning. *CLD* flag is 0 if the *LWC* is below 20 μm, 1 if the *LWC* is between 20 and 100 μm, 2 if the *LWC* is between 100 and 200 μm and 3 if the *LWC* is greater than 200 μm. Hereinafter these will be referred to as the AMC products.

III. METHODOLOGY

In this Section, we describe the methodology for the *SSI* computation and its application. *SSI* is defined as the ratio between the brightness temperatures observed at 23.8 and 31.4 GHz, and it is employed to discriminate among line of sight (LOS) sky conditions (clear-sky, cloudy or rainy) to select the most reliable path delay retrievals in the tropospheric correction algorithm. The discriminating aspects of performance within *SSI* were tested in previous works [18, 26] with radiometric observations mainly at zenith or at fixed elevation angles [27]. Here, the method has been further developed for its application to deep-space probes radio tracking, with *SSI* being parameterized as a function of the elevation angle to be commanded by a radiometer equipped with a steering mechanism.
The procedure that we followed for *SSI* implementation needs ancillary information from radiosonde observations (RAOBs), which are described in §III.A. The *SSI* implementation and the validation of the methodology are described in §III.B, and SSI development is given in §III.C.

A. RAOBs

Radiosonde observations (RAOBs) have been used in this study to parameterize *SSI* as a function of the elevation angle, as described in §III.B. RAOBs were acquired at the closest RAOB station to Goldstone, (WMO 72381, at Edwards CA/AFB) from 1994 to 2014, and are available from the NOAA/Earth System Research Laboratory (ERSL) Global Systems Division archive [28]. RAOB

profiles have been additionally quality-controlled to keep only the highest quality profiles. The quality-control process is described in [29].
A large database of simulated radiometric brightness temperature observations (T_{BS}) at the AWVR frequency channels was generated at elevation angles from 15 to 90 degrees with 5-degree interval, by using a radiative transfer algorithm [30]. The model proposed by Rosenkranz [31-32] for gaseous absorption has been used in applying the radiative transfer scheme and the cloud model in [33] was used to generate cloud liquid water profiles. The resulting database contains 6469 profiles and it spans the entire range of the expected path delay, water vapor and cloud liquid water conditions.

B. Metodology description

The procedure is summarized as follows: i) *SSI* values are computed from simulated radiometric brightness temperatures and the elevation-dependent *SSI* threshold (reference value) between clear and cloudy sky conditions is determined; ii) *SSI* values computed from AWVR measurements acquired during the deep space tracking phase are compared with the proper reference value to discriminate the clear-sky measurements and to trigger the use of the AMC calibration; iv) the OD solution is computed considering the two possible troposphere calibration techniques (TSAC and AMC); and v) the range rate residuals are compared among the two cases and the indications issued from both the *SSI* screening and the AMC products.
A crucial aspect in our work is the application of the *SSI* index to evaluate the advantage of using the AMC calibration when the instantaneous *SSI* is below the *SSI* threshold. We base our analysis on the comparison of the orbital solution of the selected flybys in terms of range rate residuals (mm/s) obtained by the Cassini Doppler observables. The use of the range rate residuals rather than the Doppler ones is preferred because the Cassini radio science communication link operates in both X-band and Ka-band. In order to process both the collected observables, the two Doppler values are scaled by their corresponding factors to the range rate: the frequency independent term, which maintains all the information available in the Doppler observables. Then, we compare the range rate residuals root mean square (RMS) when the observables are calibrated with TSAC and when they are calibrated with AMC. A reduction of the RMS residual value indicates a more accurate calibration. For the comparison we assume that the setup used for the OD solution differs only by the use of the tropospheric calibration.

C. SSI developement

The *SSI* definition and computation are fully described in [18]. Here, for an overview of the approach, the major features are discussed. The basic assumption is that in clear-sky conditions i.e. when the contribution to the thermal noise is mainly due to the water vapor (besides the small effect of dry gases), the ratio between ground-based brightness temperature measurements collected around 20-30 GHz, respectively for this radiometer at 31.4 GHz and 23.8 GHz, almost show a linear relationship. As the amount of water content increases or a liquid phase appears, this linear relationship does not hold and the two line frequencies accord a different weight to the water vapor and the cloud liquid along the path. Hence, the ratio $T_B(f_2,\theta)/T_B(f_1,\theta)$ of concurrent radiometric measurements depends on the thermodynamic state of the atmosphere. *SSI* definition is given in eq. (1) [18] by:

$$SSI(\theta) = \frac{T_B(31.4,\theta) - c_0(\theta)}{T_B(23.8,\theta)} \tag{1}$$

where $T_B(23.8,\theta)$ and $T_B(31.4,\theta)$ are the brightness temperatures at frequency channel f_1= 23.8 GHz and f_2= 31.4 GHz measured at elevation angle θ.
For the Goldstone site, the zenithal *SSI* values range from 0.28 up to above 1, depending on the atmospheric conditions. In clear-sky conditions, although SSI is not constant, it changes slowly with the water vapor content and a threshold value (= 0.3 in our work) is easy identified. As the

atmospheric conditions change and some liquid clouds are in the observation path, *SSI* values rapidly increase due to the fact that the channel centered at 31.4 GHz is more sensitive to liquid water than the channel centered at 23.8 GHz. Under rainy conditions, both channels are near the saturation and their ratio, *SSI*, is close to 1 or above.

The computation of *SSI* requires the knowledge of the coefficient c_0, which can be calculated by using either simulated or measured $T_B(f,\theta)$ [26] as the intercept of the best fit performed on couples of ($T_b(23.8)$,$T_b(31.4)$) strictly referred to clear-sky conditions. From a radiative point of view, c_0 accounts for the atmospheric dry contribution along the observed path. In this study, the parameterizations of both the coefficient $c_0(\theta)$ and the clear-sky $SSI(\theta)$ as a function of elevation angle are addressed, to extend the application of *SSI* to tracking radiometers. As AWVR and DSS antenna track the Cassini spacecraft, measurements are taken at several different observation angles ($6° < \theta < 78°$), and *SSI* values need to be computed accordingly from $T_{BS}(f,\theta)$ and angle-dependent $c_0(\theta)$. The objective is to develop theoretical reference values for $c_0(\theta)$ and $SSI(\theta)$ and to use these values as a threshold for actual *SSI* computations from the AWVR radiometer. Then, an actual *SSI* value below the threshold identifies clear sky conditions along the observation path and triggers the use of AMC path delay retrieval in the OD. The parameterization of both $c_0(\theta)$ and $SSI(\theta)$ expressions was derived from a statistical analysis performed on the simulated brightness temperature dataset described in §III.A. The dependency on the elevation angle has been expressed in terms of the air mass (AM) coefficient $AM=1/\sin(\theta)$, with the refinements given in [34] to account for the Earth curvature at low elevation angles:

$$AM' = AM - h \cdot AM\left(AM^{\,2} - 1\right)/R_e \tag{2}$$

being R_e=6370.95 km and h=1.9 km the Earth radius and an equivalent height value respectively. The relationship between the pairs of simulated T_{BS} at 23.8 and 31.4 GHz under the hypothesis of clear sky conditions can be modeled through a linear relationship with fairly good agreement in the elevation angular span comprised between 25 deg and 90 deg. At low elevation angles, a non-linear behavior (quadratic) appears on top of the linear one for high water vapor values as elevation diminishes and, correspondingly, the sensitivity of the brightness temperature to water vapor diminishes. In terms of c_0, as it accounts for the dry contribution of the atmosphere, it was modeled as the intercept of the linear fit of the lower range of T_{BS}, i.e. the driest conditions.

The computed c_0 values are reported w.r.t. the air mass in Fig.1 (black circles) together with the quadratic fit (red line) that issues from a regression analysis over 1812 couples of brightness temperature values simulated under the driest sky conditions, i.e. $max(T_{BS}(23.8,5°))$<120 K. The expression of the quadratic fit is the following:

$$c_0(AM) = -0.08287 \cdot AM^2 + 4.7879 \cdot AM + 2.0258 \tag{3}$$

that models the computed values with a l1-norm residual $R = \sum_{1}^{1812} |\hat{c}_0 - c_0| = 0.0175$. Then, the *SSI* values were computed for all 5669 clear sky RAOBs profiles according to eq.(1). Fig. 2 reports the *SSI* values (colored dots) w.r.t. air mass together with the corresponding standard deviation (SD) values (black bars) that span from 0.013 to 0.025 at 90 deg and 5 deg, respectively. Though the *SSI* values were computed from clear sky brightness temperature values, the dispersion about an average value, at each specific elevation angle, accounts for the diverse atmospheric conditions. As expected, the greater the air mass value the higher the SD is.

The regression analysis performed on the average values evidenced the linear relationship between the SSI values and the air mass ones:

$$SSI_{clear\,sky}(AM) = 0.00445 \cdot AM + 0.2784 \tag{4}$$

that models the computed values with a l1-norm residual $R = \sum_{1}^{5669} \left| \hat{SSI} - SSI \right| = 0.0013$.

SSI can be computed similarly by using radiometric measurement alone, provided that the instrument is routinely calibrated and that the amount and quality of data are statistically representative of the atmospheric conditions of the measurement site. In our study the chosen approach for the computation of the coefficient c_0 and of the reference clear sky *SSI* value has been by using simulations from RAOBs. The choice was mainly driven by the availability of a large dataset of RAOBs, spanning a wide range of path delay, water vapor and cloud liquid water conditions, compared to a much lesser availability of radiometric measurements to be able to perform a meaningful best fit, especially at different low elevation angles. Also, using a non-linear correction term for c_0 or *SSI* may be envisaged at lower elevations (below 15 deg) for specific tracking activity activities and applications. Measurements and simulations are in good agreement as shown in Fig. 4 where four elevation angles, namely, 20, 30, 45 and 70 deg, were chosen to compare the two datasets. Due to the different dynamic range of the values represented in the four panels, they were plotted with reference to each specific scale interval.

IV. *SSI* AS RADIOMETRIC QUALITY INDEX FOR DEEP SPACE OBSERVABLES TROPOSPHERE CALIBRATION

In this section, we report the results of the analysis detailed in §III for each Cassini flyby listed in Table I. The instantaneous *SSI* value, computed as described in §III.B, is compared with the reference value resulting in a two-state quality index (above or below the threshold) that is used as an on-off indicator to envisage the use of the AMC time series. The *SSI* performance is evaluated through the comparison, pass by pass, of the so-derived range rate residuals, in terms of theirs RMS values, with those given by the TSAC calibration. Table II reports the typical parameters used to validate the OD solutions. In particular, M is the mean value of the residuals in mm/s, RMS is the root mean square of the residuals in mm/s and N is the number of points (residuals) in the pass. We report in the table the three parameters for both the AMC and TSAC solutions. In each single pass, an M value closer to zero means that there is lesser bias between the observed and the computed deep space observables. M is expected to be as close as possible to zero to assess the quality of the OD solution.

The use of different path delay calibration time series may result in a different *N* value in the two solutions from the orbit determination process, and the comparison is meaningful if the *N* difference is in the order of 1%.

We point out that in 2003, at the beginning of the tour phase of the Cassini mission, the Ka-band Translator (KAT) that allows the multi frequency link failed. This is a crucial aspect for the mission and for the radioscience experiments, because the solar plasma noise cannot be completely removed as it was initially. As described in [13] and [14] the troposphere path delay is the main source of error in the Doppler observables when the plasma noise is completely removed.

For this reason, the advantage to use a more accurate troposphere calibration technique can be less evident due to the uncalibrated plasma noise. In terms of RMS, it leads to a smaller difference between the two calibration techniques.

As can we see in Table II, comparing the *M* and *N* parameters for each flyby results that the OD solutions are comparable. The *M* values are close to zero and the *N* values are mainly the same according to the introduced and expected tolerance.

As far as the RMS values are concerned, the analysis on the computed absolute difference between the two values per flyby shows that - among the 17 analyzed cases - the AMC calibrated solutions provides a smaller RMS value in 12 cases. In addition, seven cases among those favorable ones give an improvement greater than 25% with a maximum in the order of 50% (the second pass during Titan T33 flyby). For the cases where the TSAC time series better calibrate the observables, the difference is below 10%, with only one case in the order of 20% (the second pass during Titan

T11). A further inspection indicates that the AMC fails to retrieve the path delay as the spacecraft was tracked under heavy clouds or rainy conditions (as suggested from a retrieved *LWC* above the 200 μm).

Table II is a snapshot of the use of the two calibration techniques for all available passes regardless the atmospheric conditions and the indications given by either the AMC flag products or the SSI values. The "AMC products" are provided with the automatic algorithms developed by JPL to characterize the sky status with different parameters, thus giving ancillary information about the LOS path. Namely, these are the *LWC* retrieval and the wind velocity flags as described in §II.A. Here, we compare the *SSI* and the AMC products indications for addressing the use of AMC calibration in terms of correlation between the two techniques. As far as *SSI* is concerned, an advantage of using the AMC calibration with respect to the TSAC is foreseen when the instantaneous *SSI* values from the AWVR measurements for a pass are below the *SSI* clear-sky reference. As far as AMC products, the use of AMC calibration is envisaged when all the flags are zero, the *LWC* is below the 20 μm and the wind speed is below 10 m/s.

The results of the analysis are given in Table III as a contingency table. The comparison consists in matching the "AMC products" with the *SSI* trend to analyze the correlation between the two techniques. The first column gives the flyby event. In the second column, "AMC products", two are the possible values: "A" or "T" according to the calibration suggested by the AMC flags, "AMC" or "TSAC", respectively. In the third column, "SSI", the possible labels are "Above", "Below" or "Event" and describe the instantaneous *SSI* time series with respect to the *SSI* reference. The first two terms label the value of the instantaneous *SSI* with respect to the reference one; then, "TSAC" or "AMC" are suggested accordingly. The label "Event" signals cases in which *SSI* correctly detects the sky status as clear sky or in presence of clouds, and, for the longest portion of the time, the instantaneous *SSI* is below the threshold still envisaging the use of the AMC calibration. The fourth column reports the meteorological conditions during the passes in the cases where clouds are present. The column "Preferred Calibration" gives the calibration method that provided the lower RMS as listed in Table II. The main result of our analysis is reported in the column "Validation". Here we use the label: i) "SSI", if the *SSI* correctly envisaged the most accurate calibration, TSAC or AMC according to the status of the sky; ii) "AMC products", if the correct prevision is done by the AMC flag products; iii) "Both" when both techniques agree in the suggested calibration; iv) "none" if none of them succeed in suggesting the most accurate calibration to be applied.

As expected, in most cases the two techniques agree, meaning that both the *SSI* and the AMC products choose correctly between the two systems (AMC or TSAC) the one that better calibrates the observables. At a deeper insight, it results that in two specific cases, Titan_T68 and Enceladus_E12, *SSI* correctly indicates the use of the TSAC with respect to the AMC products. In three other cases, identified as "Event" in the *SSI* column, *SSI* envisaged the use of AMC calibration as the most appropriate technique. Moreover, there are three further cases for which none of the two indicators suggested the use of the AMC calibration, even if its use would have resulted in a better calibration, i.e. a smaller RMS value. Nevertheless, especially for the cases of Rhea_4, the difference in the residuals RMS is minimal probably related to the extremely windy conditions. These cause an increase in the antenna mechanical noise that overwhelms the troposphere error [12]. In the case of the Saturn rev68, the relative humidity (*RH*) time series reported values in the order of 60% (very high for the remote area of the DSS 25) and the *CLD* flag detected *LWC* values below the 20 μm. In this case, both *SSI* and AMC were above the threshold and the use of AMC was not envisaged, although it was demonstrated that AMC provided a better RMS. This case, together with the three "Event" cases successfully calibrated by using AMC, may suggest that AMC could accurately calibrate the troposphere even in presence of small amounts of liquid, although in our analysis, only the clear and the non-clear sky conditions were discriminated. If this is the case, the *SSI* threshold could be modified to include a certain level of liquid water.

With respect to the available *CLD* flag from the AMC products, the advantage of using the *SSI* is that it allows discriminating radiometric measurements without the need of *LWC* retrieval algorithms and other instruments measurements rather than AWVR. This aspect can be crucial in particular if some of the components are affected by malfunctioning. This specific situation happened in 2011-2012, when the MTP unit of the AMC installed in Goldstone experienced a fault that affected the flag time series. In such a case, the combined use of the AMC products and the *SSI* may give further indication in that sense.

V. Conclusions

In this work, the *SSI* criterion was extended to be used with a steerable radiometer, during deep-space tracking, with the purpose of addressing the effectiveness of the AMC-based calibration. Our analysis showed that i) *SSI* is a useful tool supporting the use of microwave radiometers for the calibration of Doppler observables during deep space tracking experiments, while ii) the improvements (in the form of decrease of the RMS values of the Doppler residuals) in the orbit determination process demonstrated the validity of using accurate tropospheric path-delay estimates from AWVR measurements (AMC-based calibration) in clear-sky conditions. The advantages of using *SSI* are manifold:

1) *SSI* approach is suitable for a real-time, automatic, and easy-to-use procedure for employing radiometric data.

2) In deep-space tracking and other applications using microwave radiometers, often concurrent measurements from additional and/or ancillary instruments aid to the screening of the diverse atmospheric conditions. This issue is even more relevant on slant path, when such information is often not available. The *SSI* method relies on radiometric measurements alone to accurately discriminate between atmospheric conditions on the slant path.

3) In the observable calibration procedure, the computation of the *SSI* and its correlation with the "AMC products" helped to promote the use of the AMC calibration during clear sky conditions. In this case, before processing the deep space observables in the OD software, *SSI* can also be useful in evaluating the behavior of the AMC time series.

4) Theoretical c_0 and *SSI* values can in principle be computed from MWR measurements when RAOBs are not available, showing that the method is fully stand-alone.

5) *SSI* can be computed at different pairs of frequencies, sensitive to water vapor and cloud liquid water in the atmosphere, respectively. For instance, frequency channels at 30 GHz or 90 GHz, as found in commercial radiometers, could be used to replace the 31.4 GHz channel. Similar considerations also apply to the 23 GHz channel although this frequency is preferred as it is better suitable for the integrated water vapor estimate.

VI. Acknowledgment

The authors wish to acknowledge the Jet Propulsion Laboratory's Radio Science Systems Group for the delivery of the Advanced Media Calibration data. Also, they wish to thank Prof. Luciano Iess, Dr. Marzia Parisi, Dr. Stefano Finocchiaro (University La Sapienza, Rome, Italy) and Dr. Marco Zannoni (University of Bologna, Italy) for the computation of the OD solutions.

VII. References

[1] X. Xie, U. Löhnert, S. Kneifel und S. Crewell, "Snow particle orientation observed by ground-based microwave radiometry," *J. Geophys. Res.,* Vol. 117, D02206, 2012, pp. 12, DOI: 10.1029/2011JD016369.

[2] E. F. Campos, R. Ware, P. Joe and D. Hudak, “Monitoring water phase dynamics in winter clouds”, *Atmos. Res*., Vol. 147–148, 2014, pp. 86–100, DOI: 10.1016/j.atmosres.2014.03.008.

[3] D. Cimini, M. Nelson, J. Güldner, and R. Ware, “Forecast indices from ground-based microwave radiometer for operational meteorology,” *Atmos. Meas. Tech. Discuss*., Vol. 7, pp. 6971-7011, 2014.

[4] C. Mallet and J. Lavergnat, “Beacon calibration with a multifrequency radiometer,” *Radio Sci.,* Vol. 27, No.5, pp. 661-680, 1992.

[5] V. Mattioli, F.S. Marzano, S. Crewell, G. Carrie, U. Löhnert, D. Cimini, E. Fionda, A. Martellucci, “Instruments, Data and Techniques for the Assessment of the Atmospheric Noise Emission in Satcom Ground Stations”, Proc. of 6th European Conference on Antennas and Propagation (Eucap 2012), Prague, 26-30 March 2012, pp. 76 – 80.

[6] Keihm S. J. and K. A. Marsh, “Advanced Algorithm and System Development for Cassini Radio Science Tropospheric Calibration,” The Telecommunications and Data Acquisition Progress Report 42-127, 1996, Jet Propulsion Laboratory, Pasadena, California, pp. 1–20.

[7] K. Ebell, E. Orlandi, A. Hünerbein, U. Löhnert und S. Crewell, “Combining ground and satellite based measurements in the atmospheric state retrieval: Assessment of the information content, *J. Geophys. Res.*, Vol.18, pp. 6940–6956, 2013.

[8] M. P. Cadeddu, J. C. Liljegren, and D. D. Turner, “The atmospheric radiation measurement (ARM) program network of microwave radiometers: instrumentation, data, and retrievals” *Atmos. Meas. Tech.*, Vol. 6, Issue 9, 2013, pp.2359-2372. DOI: 10.5194/amt-6-2359-2013.

[9] D. D. Turner, M. P. Cadeddu, U. Löhnert, S. Crewell, and A. M. Vogelmann, “Modifications to the Water Vapor Continuum in the Microwave Suggested by Ground-Based 150-GHz Observations,” *IEEE Trans. Geosci. Rem. Sens.*, Vol. 47, Issue 10, pp. 3326-3337, 2009.

[10] B. Bertotti, L. Iess, and P. and Tortora, “A test of general relativity using radio links with the Cassini spacecraft”, *Nature*, Vol. 425, pp. 374–376, September, 2003.

[11] V. Mattioli, E. R. Westwater, S. Gutman, and V. Morris, “Forward Model Studies of Water Vapor using Scanning Microwave Radiometers, Global Positioning System and Radiosondes during the Cloudiness Inter-Comparison Experiment,” *IEEE Trans. Geosci. Rem. Sens.*, vol. 43, Issue 5, pp. 1012–1021, May, 2005.

[12] D. D. Turner, S. A. Clough, J. C. Liljegren, E. E. Clothiaux, K. E. Cady-Pereira, and K. L. Gaustad, “Retrieving liquid water path and precipitable water vapor from the Atmospheric

Radiation Measurement (ARM) microwave radiometers," *IEEE Trans. Geosci. Rem. Sens*., vol. 45, no. 11, Nov. 2007.

[13] L. Iess, M. Di Benedetto, N. James, M. Mercolino, L. Simone and P. Tortora, "Astra: Interdisciplinary study on enhancement of the end-to-end accuracy for spacecraft tracking techniques", *Acta Astronautica*, Vol. 94, Issue 2, February 2014, pp. 699-707, ISSN 0094-5765, http://dx.doi.org/10.1016/j.actaastro.2013.06.011.

[14] P. Tortora, S. Crewell, G. Elgered, A. Graziani, P. Jarlemark, M. Lanucara, U. Löhnert, A. Martellucci, M. Mercolino, T. Rose and J. Schween, "Instruments, Data and Techniques for the Assessment of Tropospheric Noise in Deep Space Tracking", Proceedings of the 6th European Conference on Antennas and Propagation (EUCAP 2012), Prague, Czech Republic, 26-30 March 2012.

[15] P.Tortora, L.Iess, J.J.Bordi, J.E.Ekelund and D.C.Roth: "Precise Cassini navigation during solar conjunctions through multifrequency plasma calibrations" *J. Guid., Control Dyn.*, Vol. 27, Issue 2, 2004, pp. 251-257.

[16] Y.E. Bar-Sever, C.S. Jacobs, S. Keihm, G. E. Lanyi, C. J. Naudet, H. W. Rosenberger, T. F. Runge, A. B. Tanner, Y. Vigue-Rodi, "Atmospheric Media Calibration for the Deep Space Network," *Proceedings of the IEEE* , vol.95, no.11, pp.2180-2192, Nov. 2007 doi: 10.1109/JPROC.2007.905181.

[17] A. B. Tanner and A. L. Riley, "Design and performance of a high-stability water vapor radiometer," *Radio Sci.*, Vol. 38, No 3, 8050, doi:10.1029/2002RS002673, 2003.

[18] A.V. Bosisio, E. Fionda, P. Basili, G. Carlesimo, A. Martellucci, "Identification of rainy periods from ground-based microwave radiometry", *Eur. J. Rem. Sens.*, Vol. 45, pp. 41-50, 2012, doi: 10.5721/EuJRS20124505.

[19] L. Iess, R. A. Jacobson, M. Ducci, D. J. Stevenson, J. I. Lunine, J. W. Armstrong, S. W. Asmar, P. Racioppa, N. J. Rappaport, and P. Tortora, "Tides of Titan", *Science*, Vol. 337, 2012, p. 457.

[20] L. Iess, D.J. Stevenson, M. Parisi, D. Hemingway, R.A. Jacobson, J.I.Lunine, F. Nimmo, J.W. Armstrong, S. W. Asmar and M . Ducci, "The Gravity Field and Interior Structure of Enceladus", *Science,* Vol. 344 (6179) , 2004, pp. 78-80. DOI 10.1126/science.1250551.

[21] N. D. Panagiotacoupulos, J. W. Zielenbach, and R. W. Duesing, "An introduction to JPL's orbit determination program" Pasadena, CA: Jet Propulsion Laboratory, National Aeronautics and Space Administration, 1974.

[22] T. D. Moyer, “Formulation for Observed and Computed Values of Deep Space Network Data Types for Navigation”, John Wiley & Sons, Inc., Hoboken, New Jersey, 2003.

[23] Webb, F. H., and J. F Zumberge, “An introduction to GIPSY/ OASIS-II,” JPL Publication D-11088, Jet Propulsion Laboratory, Pasadena, California, 1997.

[24] G. M. Resch, “Inversion Algorithms for Water Vapor Radiometers Operating at 20.7 and 31.4 GHz”, TDA Prog. Report 42-76, pp. 12-26, Oct. 1983.

[25] S. J. Kehim and K. A. Marsh, “New model-based Bayesian inversion algorithm for the retrieval of wet troposphere path delay from radiometric measurements”, *Radio Sci.*, Vol. 33, Issue 2, 1998, pp. 411-419.

[26] A.V. Bosisio, P. Ciotti, E. Fionda and A. Martellucci, “A sky status indicator to detect rain-affected atmospheric thermal emissions observed at ground,” *IEEE Trans. Geosci. Rem. Sens*, Vol. 51, No. 9, pp. 4643-4649, 2013.

[27] V. Mattioli, A. Graziani, P. Tortora, A. V. Bosisio, and L. Castanet, “Analysis and improvements of methodologies for discriminating atmospheric conditions from radiometric brightness temperatures”, Proc. of the 7th European Conference on Antennas and Propagation (EuCAP), Gothenburg, Sweden, 8-12 April 2013, pp. 1392 - 1396.

[28] B. E. Schwartz, and M. Govett, “A hydrostatically consistent North American Radiosonde Data Base at the forecast Systems Laboratory, 1946-present”, NOAA Technical Memorandum ERL FSL-4, 1992, NTIS PB 112225.

[29] V. Mattioli, E. R. Westwater, D. Cimini, J. C. Liljegren, B. M. Lesht, S. I. Gutman, and F. J. Schmidlin, "Analysis of Radiosonde and Ground-Based Remotely Sensed PWV Data from the 2004 North Slope of Alaska Arctic Winter Radiometric Experiment", *J. Atmos. Ocean. Tech*., vol. 24, Issue 3, pp. 415-431, Mar. 2007, doi: 10.1175/JTECH1982.1.

[30] J. A. Schroeder and E. R. Westwater, “Users’ guide to WPL microwave radiative transfer software,” *NOAA Tech. Rpt. ERL-219 WPL-213*, 1991, 84 pp., NOAA/Environmental Research Laboratories, Boulder ,CO.

[31] P. W. Rosenkranz, “Water vapor microwave continuum absorption: a comparison of measurements and models,” *Radio Sci.,* vol. *33* Issue 4, 1998, pp. 919–928.

[32] P. W. Rosenkranz, “Correction to water vapor microwave continuum absorption: a comparison of measurements and models,” *Radio Sci.*, Vol. *34*, Issue 4, 1999, p. 1025.

[33] V. Mattioli, P. Basili, S. Bonafoni, P. Ciotti, and E. R. Westwater, "Analysis and improvements of cloud models for propagation studies", *Radio Sci.,* Vol. 44, RS2005, Mar 2009, doi:10.1029/2008RS003876.

[34] Y. Han and E. R. Westwater, "Analysis and improvement of tipping calibration for ground-based microwave radiometers," *IEEE Trans. Geosci. Rem. Sens.,* vol. 38, no. 3, 2000, pp. 1260–1276.

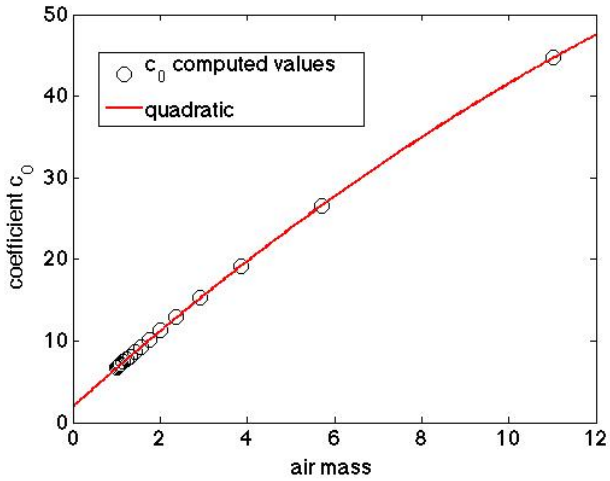

Fig. 1– The quadratic behavior of coefficient c_0 (red line) is derived from the regression fit over the driest 1812 c_0 values (black circles) computed from simulated brightness temperatures RAOBs based.

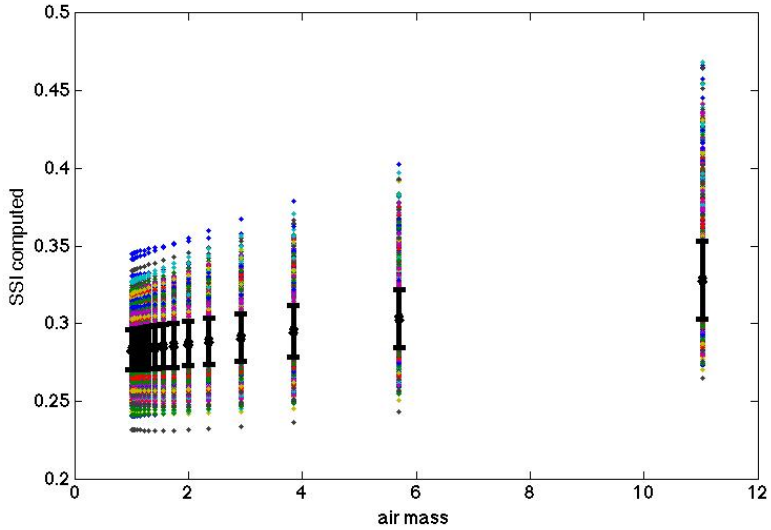

Fig. 2 - The SSI values (coloured dots) with the associated standard deviation values (black bars) versus air mass. The SSI values are strictly associated to the clear sky conditions as derived from the RAOBs dataset.

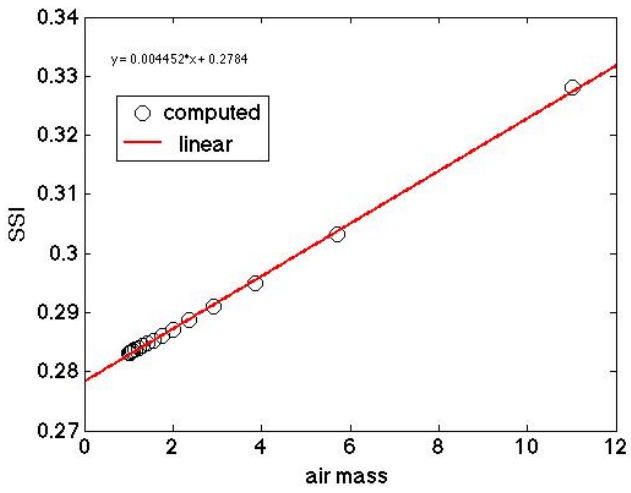

Fig. 3 - The average clear sky SSI values (black dots) w.r.t the air mass. The red lines represent the linear regression best fit.

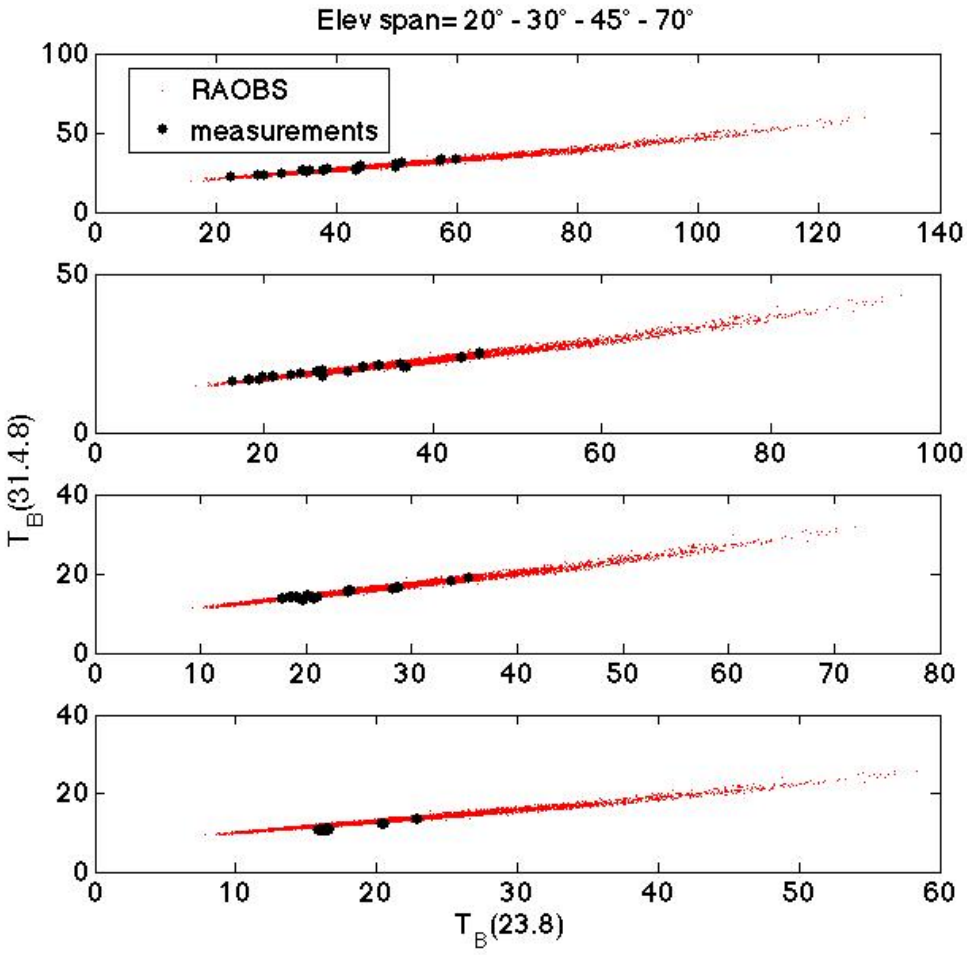

Fig. 4 - Scatter diagram of $T_b(31.4)$ versus $T_b(f)(23.8)$ simulated values from RAOBs dataset (red dots) and measured one (black dots) at 20, 30, 45 and 70 deg from top to bottom.

TABLE I. LIST OF 10 SELECTED GRAVITATIONAL FLY-BYS

Name	Flyby date	Number of passes
Enceladus_E12	30 November 2010	1
Iapetus	10 September 2010	1
Rhea_4	9 March 2013	3
Saturn_Rev28	09 September 2006	1
Saturn_Rev68	17 May 2008	1
Titan_T11	27 February 2006	3

Titan_T22	28 December 2006	2
Titan_T33	29 June 2007	3
Titan_T45	31 July 2008	1
Titan_T68	20 May 2010	1

TABLE II. RANGE RATE RESIDUALS ROOT MEAN SQUARE AND MEAN VALUE OBTAINED WITH TSAC AND AMC CALIBRATION

	#	TSAC			AMC		
		M [mm/s]	RMS [mm/s]	N	M [mm/s]	RMS [mm/s]	N
Enceladus_E12	1	9,50E-05	0,004194	271	3,81E-05	0,004288	269
Iapetus	1	3,10E-03	0,111748	132	4,72E-03	0,077673	131
Rhea_4	1	5,32E-04	0,022363	330	4,19E-05	0,020456	328
	2	5,68E-03	0,030391	153	7,16E-03	0,031732	151
	3	-3,32E-04	0,021714	331	4,01E-04	0,019662	331
Saturn_Rev28	1	9,61E-06	0,033716	371	1,50E-04	0,029961	371
Saturn_Rev68	1	1,17E-05	0,026014	245	3,76E-05	0,021044	245
Titan_T11	1	3,19E-04	0,034045	314	7,64E-04	0,022472	313

	2	1,43E-05	0,025494	437	1,44E-03	0,031234	437
	3	2,02E-04	0,024612	385	1,11E-04	0,017001	383
Titan_T22	1	8,52E-05	0,044444	401	2,43E-03	0,024772	399
	2	4,83E-04	0,02274	197	2,73E-03	0,016832	197
Titan_T33	1	1,32E-03	0,037659	453	2,88E-03	0,031581	499
	2	2,65E-04	0,048616	207	1,31E-03	0,024167	207
	3	2,11E-03	0,049268	389	2,70E-03	0,02706	447
Titan_T45	1	2,15E-03	0,067852	504	8,58E-03	0,075971	504
Titan_T68	1	3,41E-03	0,03939	443	4,23E-03	0,040425	443

TABLE III. RESIDUALS ESTIMATION: CONTINGENCY TABLE

	AMC products	**SSI**	**Notes and events**	**Preferred calibration**	**Validation**
Enceladus_E12	A	Above		TSAC	SSI
Iapetus_S33	A	Below		AMC	Both
Rhea_4	T	Above	Cloudy and windy	AMC	none
	T	Above	Cloudy and windy	TSAC	Both
	T	Above	Cloudy and windy	AMC	none
Saturn_Rev28	A	Below		AMC	Both
Saturn_Rev68	T	Above		AMC	none
Titan_T11	T	Event	Clouds	AMC	SSI
	T	Above	Clouds	TSAC	Both
	A	Event	Clouds	AMC	Both
Titan_T22	T	Event	Heavy clouds	AMC	SSI
	T	Event	Heavy clouds	AMC	SSI
Titan_T33	A	Below		AMC	Both
	A	Below		AMC	Both
	A	Below		AMC	Both
Titan_T45	T	Above	Clouds	TSAC	Both
Titan_T68	A	Above		TSAC	SSI